Applications in Engineering Science 8 (2021) 100068

Contents lists available at ScienceDirect

Applications in Engineering Science

journal homepage: www.sciencedirect.com/journal/applications-in-engineering-science

Simple shear flow of a Herschel-Bulkley fluid with wall slip above a threshold stress

Georgios C. Georgiou

Department of Mathematics and Statistics, University of Cyprus, PO Box 20537, Nicosia 1678, Cyprus

ARTICLE INFO

Keywords:
Wall slip
Herschel-Bulkley model
Navier slip
Slip yield stress
Rheometry

ABSTRACT

The simple shear flow of Herschel-Bulkley fluids is analyzed, under the assumption that wall slip occurs at both plates above a characteristic wall shear stress, the slip yield stress. The latter critical value is usually lower than the yield stress of viscoplastic materials exhibiting wall slip. The effects of wall slip and the slip yield stress on the apparent flow curve, i.e. the plot of the shear stress vs the apparent shear rate, are investigated. With non-viscoplastic fluids, the flow curve is gap-independent below the slip yield stress. Above a critical apparent shear rate at which the slip yield stress is exceeded, a plateau zone is encountered, and then the flow curve becomes gap dependent. Viscoplastic materials remain at rest for stresses below the slip yield stress, slide unyielded for stresses between the slip yield stress and the yield stress, at half the velocity of the moving plate, and yield and slip for stresses above the yield stress. Hence, the apparent flow curve exhibits an initial plateau corresponding to slip yield stress, followed by a rapid-growth gap-dependent part and a second plateau corresponding to the yield stress, and then approaches asymptotically its zero-slip-yield-stress counterpart. This behavior describes well certain rheometric experiments on concentrated suspensions and pastes.

1. Introduction

Non-Newtonian fluids, such as biological gels and tissues, are prone to slip (Hatzikiriakos 2012,2015; Ewoldt et al., 2015). A consequence of wall slip in rheometric experiments is that the actual shear rate does not coincide with the apparent shear rate. The difference between true and apparent shear rate depends on the geometry, e.g. on the gap size in the case of simple shear flow and on the diameter in capillary flow. The errors in the determination of rheological parameters may sometimes rise to an order of magnitude (Poumaere et al., 2014). Hence, wall slip needs to be taken into account, in order to obtain reliable estimates of the rheological parameters (Hatzikiriakos 2012,2015; Ewoldt et al., 2015).

The effects of wall slip in rheometry have been investigated since the early 1930s. Schofield and Scott Blair (1931) studied slip in capillary flow and derived explicit formulae to calculate the slip velocity from experimental data for any fluid. Mooney (1931) also derived explicit formulae relating the slip velocity to the wall shear stress for capillary and circular Couette data that require measurements at three different diameters. Much later, Yoshimura and Prud'homme (1988) proposed a different analysis of the Couette geometry that requires only two measurements. They also provided wall slip corrections for parallel disk viscometers. Medina-Bañuelos et al. (2017) also investigated the errors caused by wall slip in tangential annular (Couette) flow of a viscoplastic microgel.

Wall slip effects are more pronounced in the case of viscoplastic materials, i.e. materials exhibiting yield stress (Bertola et al., 2003; Chaparian and Tammisola, 2021; Cloitre and Bonnecaze, 2017; Meeker et al., 2004a; Chaparian and Tammisola, 2021). Below the yield stress these materials may slide in the presence of slip (Damianou et al., 2019; Chaparian and Tammisola, 2021), in which case the apparent shear rate is finite while the actual one is zero.

The objective of the present paper is to analyze the implications of wall slip on the apparent flow curve resulting from simple shear experiments on Herschel-Bulkley fluids (Herschel and Bulkley, 1926), whose constitutive equation has the following scalar form:

$$\begin{cases} \dot{\gamma} = 0, & \tau \le \tau_0 \\ \tau = \tau_0 + k\dot{\gamma}^n, & \tau > \tau_0 \end{cases} \tag{1}$$

where τ is the shear stress, $\dot{\gamma}$ is the shear rate, τ_0 is the yield stress, k is the consistency index, and n is the flow index or shear thinning exponent. The Bingham-plastic model is recovered by setting $n = 1$ and replacing k by the plastic viscosity μ. The power-law model is also the special case of Eq. (1) when $\tau_0 = 0$, i.e.

E-mail address: georgios@ucy.ac.cy.

https://doi.org/10.1016/j.apples.2021.100068
Received 5 July 2021; Received in revised form 7 September 2021; Accepted 25 September 2021
Available online 28 September 2021
2666-4968/© 2021 Published by Elsevier Ltd. This is an open access article under the CC BY-NC-ND license (http://creativecommons.org/licenses/by-nc-nd/4.0/).

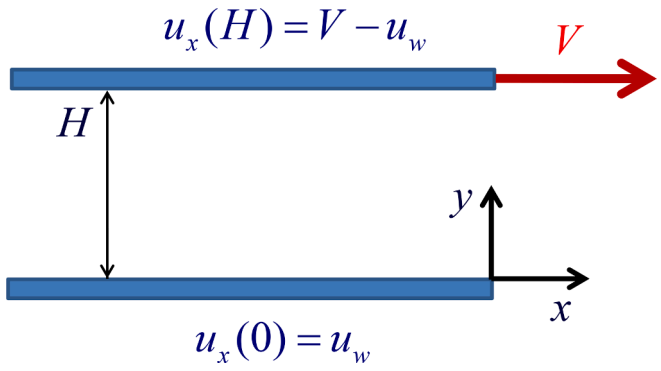

Fig. 1. Geometry and boundary conditions of simple shear flow with slip at both walls.

$$\tau = k\dot{\gamma}^n \tag{2}$$

Setting $n = 1$ and $k = \mu$, one gets the Newtonian model, $\tau = \mu\dot{\gamma}$, where μ represents the shear viscosity.

In the present work we consider wall slip that occurs when a critical wall shear stress, the slip yield stress, is exceeded (Ballesta et al., 2008, 2012; Damianou et al., 2019; Chaparian and Tammisola, 2021). More specifically, the following slip law is employed:

$$\begin{cases} u_w = 0, & \tau_w \le \tau_c \\ \tau_w = \tau_c + \beta u_w^s, & \tau_w > \tau_c \end{cases} \tag{3}$$

where u_w is the slip velocity, i.e. the relative velocity of the fluid particles to that of the wall, τ_w is the wall shear stress, τ_c is the slip (or sliding) yield stress, β is the slip coefficient and s is the slip exponent. The classical Navier slip (Navier, 1827) is recovered when $\tau_c = 0$ and $s = 1$.

$$\tau_w = \beta u_w \tag{4}$$

The no-slip condition corresponds to $\beta \to \infty$; hence, wall slip is enhanced as β is reduced. The condition (3) is also known as the stick/slip condition or the no-slip/Navier-slip condition (Blechta et al., 2020).

In the case of polymers, the critical shear stress for the onset of slip is linearly correlated to the work of adhesion of the corresponding polymer wall interface (Hill et al., 1991; Anastasiadis and Hatzikiriakos, 1998), suggesting that slip is a result of an adhesive failure of the interface. In most experimental reports on viscoplastic materials, such as pastes, gels and colloidal suspensions, the slip yield stress is smaller than the yield stress, $\tau_c < \tau_0$ (Damianou et al., 2019; Meeker et al., 2004a, 2004b, and references therein).

In the past few years, many studies of viscoplastic flows with wall slip and non-zero slip yield stress have been reported. In their comprehensive study of the slip and flow of concentrated colloidal suspensions, Ballesta et al. (2012) considered the parallel plate flow of a Herschel-Bulkley fluid with $n = 1/2$ and the special case of the slip law (3) with $s = 1$and derived analytical solutions in the various flow regimes arising from the relative values of the slip yield stress, the yield stress, and the wall shear stress. They then used these solutions to approximate the flow in a cone-and-plate rheometer.

Damianou et al. (2014) studied the axisymmetric Poiseuille flow of a Herschel–Bulkley fluid with wall slip following a slip law with slip yield stress and identified the various steady-state regimes depending on the relative values of τ_c, τ_0 and the wall shear stress. They also solved numerically the cessation of the flow using regularized versions of the constitutive and slip equations and showed that when the slip yield stress is non-zero, slip ceases at a finite critical time and the velocity becomes flat only at complete cessation. Subsequently, Damianou et al. (2016) extended their work to the two-dimensional Poiseuille flow of a Bingham plastic in rectangular ducts. More recently, Damianou et al. (2019) analyzed the steady-state Couette flow of a Bingham-plastic with wall slip and non-zero slip-yield stress, identified the different flow regimes that arise when $\tau_c < \tau_0$, and derived analytical expressions for the velocity and the critical angular velocities defining these regimes.

The rest of the paper is organized as follows. In Section 2 the general form of the linear velocity profile in the simple shear flow of any fluid with a monotonic constitutive equation is presented, under the assumption that the same slip law applies so that the slip velocity is the same at both plates. The velocity in the gap is written in terms of the

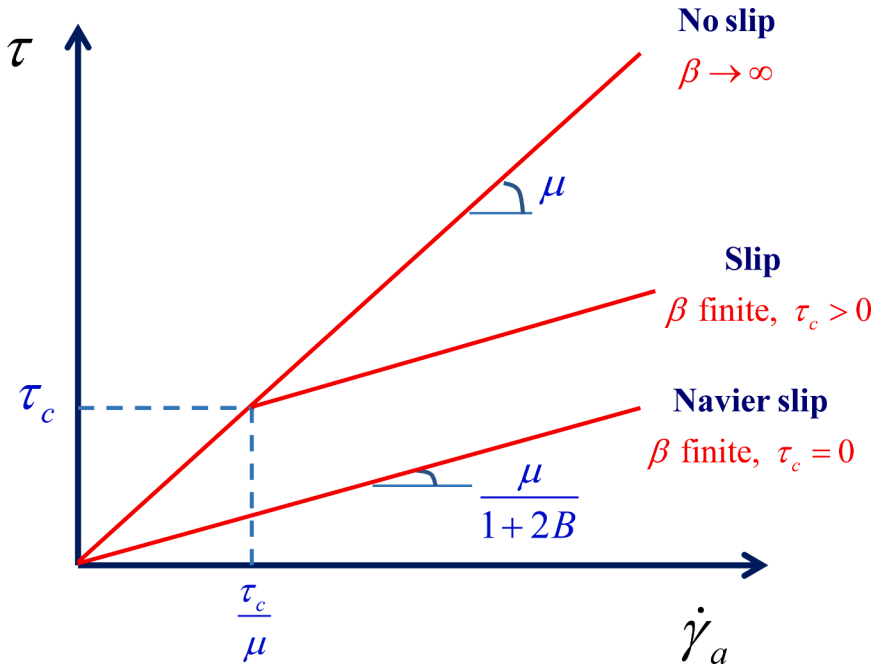

Fig. 2. Apparent flow curves of a Newtonian fluid with no-slip, Navier slip, and slip with non-zero slip yield stress. The Navier-slip flow curve is of lower slope than its no-slip counterpart. With non-zero slip yield stress, slip occurs above a critical apparent shear rate $\dot{\gamma}_{ac} = \tau_0/\mu$ and thus the flow curve consists of two branches, the first coincides with the no-slip flow curve and the second is of the same slope as the Navier-slip one.

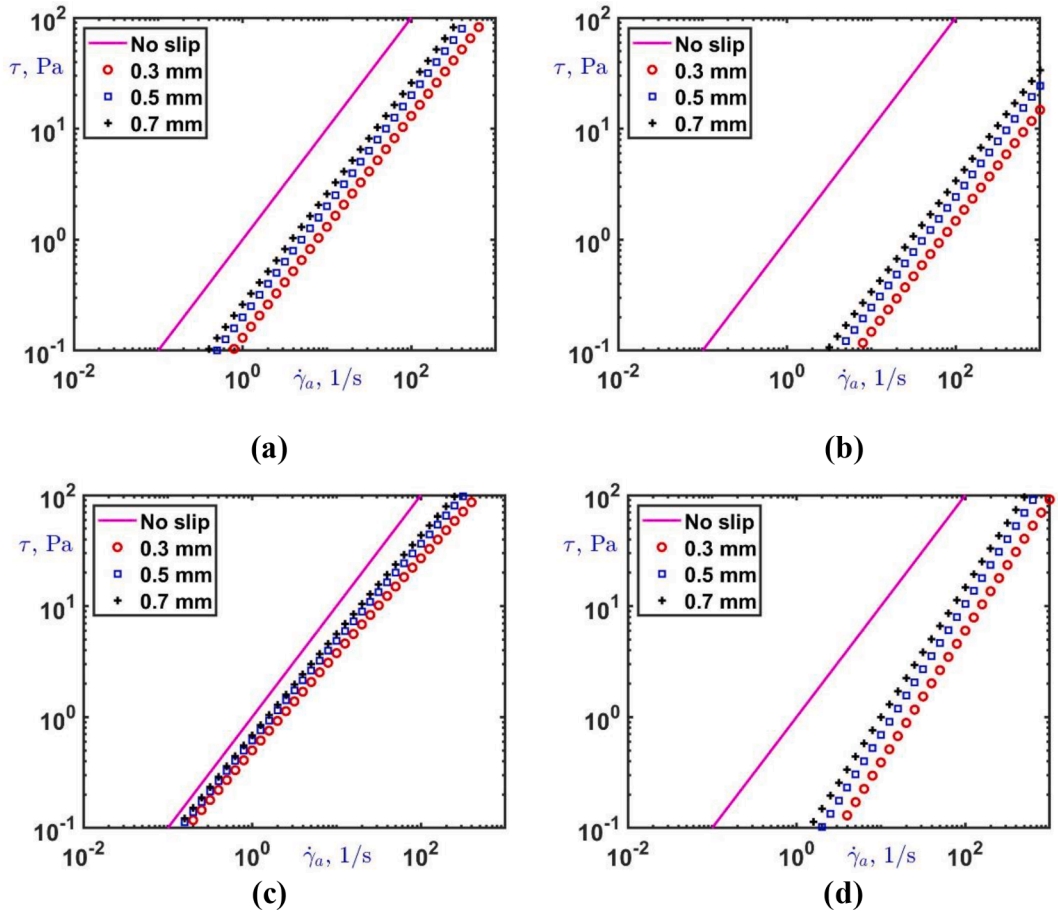

Fig. 3. Apparent flow curves obtained for a Newtonian fluid ($\mu = 1$Pa·s) and wall slip with zero slip yield stress: (a) $\beta = 1000$Pa·s/m and $s = 1$ (strong Navier slip); (b) $\beta = 100$Pa·s/m and $s = 1$ (very strong Navier slip); (c) $\beta = 1000$Pa·s$^{1/s}$/m$^{1/s}$ and $s = 0.8$; (d) $\beta = 1000$Pa·s$^{1/s}$/m$^{1/s}$ and $s = 1.2$. The flow curve corresponding to no-slip is also shown. The results for the three gap sizes do not coincide in the presence of slip; they are parallel straight lines only in the case of Navier slip ($s = 1$).

common slip velocity, which is determined numerically in the general case. In Section 3, the flows of Newtonian and power-law fluids are analyzed and analytical solutions are provided for certain values of the flow index n and the slip exponent s. To visualize the gap-size effect and facilitate the discussion, results are obtained for certain gap sizes. Finally, Herschel-Bulkley shear flows are analyzed and discussed in Section 4. It is demonstrated that using a single slip equation with non-zero slip yield stress may describe adequately experimental flow-curve data at different gap sizes where the flow curves coincide for low apparent shear rates, then they diverge, and, as the shear rate increases, they merge again approaching asymptotically the no-slip flow curve (Ewoldt et al., 2015; Moud et al., 2021a).

2. General equations

Consider the simple shear flow between parallel plates and assume that the gap distance is H and that the upper plate is moving at a constant velocity V in the x-direction, while the lower one is fixed, as illustrated in Fig. 1. It is easily deduced from the x-momentum equation that the shear stress τ_{yx} is constant and thus the velocity varies linearly with the transverse coordinate y, i.e. $u(y) = c_1 + c_2 y$, where the constants c_1 and c_2 are determined from the boundary conditions. In the absence of slip, $u(0) = 0$ and $u(H) = V$, which give the linear profile $u(y) = yV/H$. The *true* shear rate $\dot{\gamma} = du/dy$ coincides with the *apparent* shear rate $\dot{\gamma}_a = V/H$ for any fluid, which renders the flow viscometric.

To simplify the analysis, we assume that the same monotonic slip law applies along both walls (this is a reasonable assumption if the two walls are of the same material and have the same properties, e.g. roughness). Given that the shear stress is constant, the velocity profile is still linear and, since the slip law is monotonic, the slip velocities at the two walls are equal; hence the boundary conditions are $u(0) = u_w$ and $u(H) = V - u_w$ (Fig. 1). Thus, the velocity distribution is given by

$$u_x(y) = u_w + (V - 2u_w)\frac{y}{H} \tag{5}$$

and the true shear rate is

$$\dot{\gamma} = \frac{du_x}{dy} = \frac{V - 2u_w}{H} = \dot{\gamma}_a\left(1 - 2\frac{u_w}{V}\right) \tag{6}$$

The slip velocity term represents the error between the true and the apparent shear rate.

Let us now assume that the material is viscoplastic exhibiting wall slip with a finite slip yield stress, such that $0 < \tau_c \leq \tau_0$. To study the apparent flow curve, we will express the stress exerted on the upper plate, τ_w, in terms of the apparent shear rate, $\dot{\gamma}_a$. It is clear that if $\tau_w \leq \tau_c$, the plate is not moving, the material behaves as a solid, and no slip occurs. Above the slip yield stress, two flow regimes are observed with viscoplastic materials. In Regime 1 (sliding regime), i.e. when $\tau_c < \tau_w \leq \tau_0$, slip occurs but τ_w is not sufficient to yield the material. Hence, the material slides as a solid at a constant speed, which implies that the actual shear rate is zero while $\dot{\gamma}_a$ is not. As a result, the apparent flow curve shows 'apparent yielding' below the true yield stress. Since the velocity is flat, $u(y) = V - u_w = u_w$, which gives $u = u_w = V/2 = H\dot{\gamma}_a/2$. From the slip law (3) we then get:

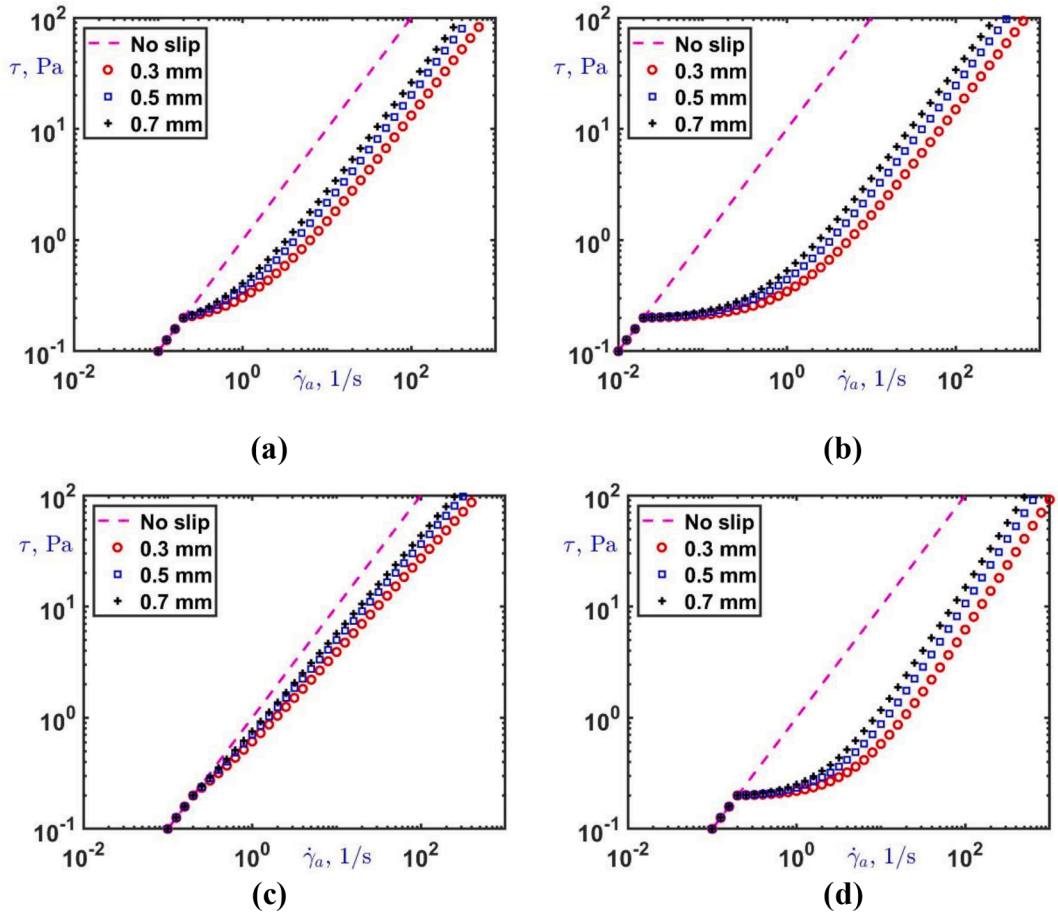

Fig. 4. Flow curves of Newtonian fluids exhibiting wall slip with non-zero slip yield- stress, $\tau_c = 0.2$Pa, and $\beta = 1000$Pa·s$^{1/s}$/m$^{1/s}$: (a) $\mu = 1$Pa·s,$s = 1$ (Navier slip); (b) $\mu = 10$Pa·s, $s = 1$; (c) $\mu = 1$Pa·s, $s = 0.8$; (d) $\mu = 1$Pa·s, $s = 1.2$. The dashed line is the flow curve corresponding to no-slip.

$$\tau_w = \tau_c + \frac{\beta H^s}{2^s}\dot{\gamma}_a^s \tag{7}$$

The critical apparent shear rate $\dot{\gamma}_{a0}$ at which $\tau_w = \tau_0$ is thus

$$\dot{\gamma}_{a0} = \frac{2}{H}\left(\frac{\tau_0 - \tau_c}{\beta}\right)^{1/s} \tag{8}$$

It should be pointed out that $\dot{\gamma}_{a0}$ is independent of the viscoplastic constitutive equation, depending only on the yield stress, the slip parameters, and the gap size H. This critical value decreases with H, in agreement with experimental observations, such as the parallel-plate experiments of Moud et al. (2021a) on kaolinite suspensions.

The constitutive equation becomes relevant in Regime 2 or yielding regime, i.e. when $\dot{\gamma}_a > \dot{\gamma}_{a0}$, where the material yields and slips at the wall. In this regime, the wall shear stress satisfies both the slip and constitutive equations and thus

$$\tau_c + \beta u_w^s = \tau_0 + k\dot{\gamma}^n \tag{9}$$

By means of Eqs. (6)–(8), the following non-linear equation is obtained:

$$\left(1 - 2\frac{u_w}{V}\right)^n = \frac{\beta H^s}{k\dot{\gamma}_a^n}\left[\dot{\gamma}_a^s\left(\frac{u_w}{V}\right)^s - \left(\frac{\dot{\gamma}_{a0}}{2}\right)^s\right] \tag{10}$$

which can easily be solved numerically to calculate the relative slip velocity u_w/V and then the second branch of the apparent flow curve:

$$\tau_w = \begin{cases} \tau_c + \beta H^s \dot{\gamma}_a^s / 2^s, & \dot{\gamma}_a \le \dot{\gamma}_{a0} \\ \tau_0 + k(1 - 2u_w/V)^n \dot{\gamma}_a^n, & \dot{\gamma}_a > \dot{\gamma}_{a0} \end{cases} \tag{11}$$

Note that the first branch that corresponds to the sliding regime ($\dot{\gamma}_a \le \dot{\gamma}_{a0}$) is independent of the constitutive equation and lies below the yield stress of the material. Eq. (10) can be solved analytically for certain combinations of the exponents n and s. Some of these solutions are provided below. To facilitate the discussion, we first consider the solutions for power-law fluids, i.e. of fluids with zero yield stress ($\tau_0 = 0$).

3. Power-law fluids

It is instructive to first analyze the flow of power-law fluids exhibiting slip with non-zero slip yield stress, $\tau_c > 0$. In this case, there are again two flow regimes corresponding to no-slip and slip. For $\tau_w \le \tau_c$, there is no slip ($u_w = 0$); hence, the true shear rate is measured and the apparent flow curve coincides with the true one. It is easily deduced by means of constitutive Eq. (1) that the critical apparent shear rate $\dot{\gamma}_{ac}$ at which slip occurs is

$$\dot{\gamma}_{ac} = \left(\frac{\tau_c}{k}\right)^{1/n} \tag{12}$$

Given that $\tau_0 = 0$, Eq. (10) can now be written as follows:

$$\left(1 - 2\frac{u_w}{V}\right)^n = \left(\frac{\dot{\gamma}_{ac}}{\dot{\gamma}_a}\right)^n + \frac{\beta H^s}{k}\dot{\gamma}_a^{s-n}\left(\frac{u_w}{V}\right)^s \tag{13}$$

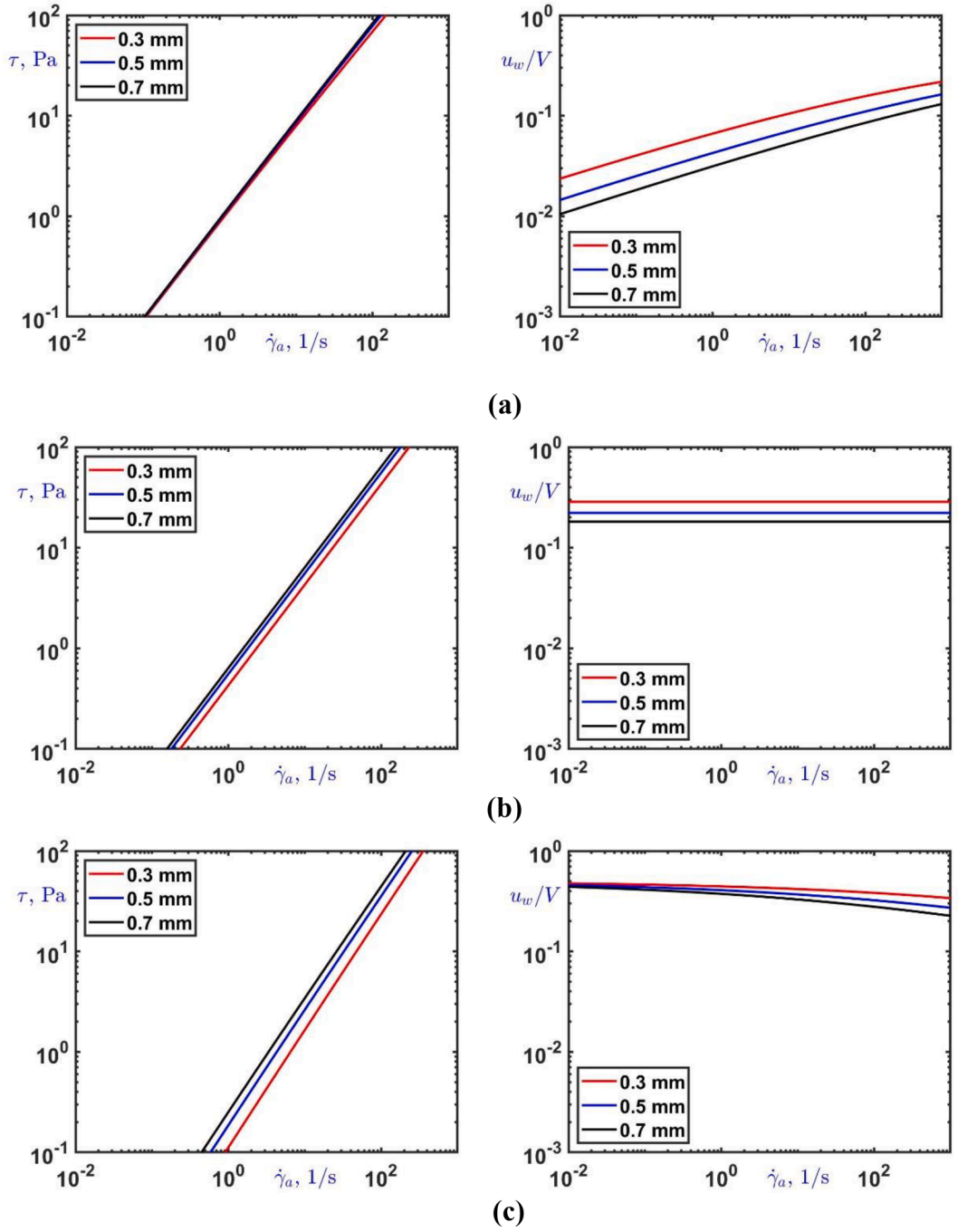

Fig. 5. Flow curves (left) and slip velocities (right) of Newtonian fluids exhibiting power-law-type slip (zero τ_c) with $\mu = 1\text{Pa}\cdot\text{s}$ and $\beta = 5000\text{Pa}\cdot\text{s}^{1/s}/\text{m}^{1/s}$: (a) $s = 0.8$; (b) $s = 1$ (Navier slip); (c) $s = 1.2$.

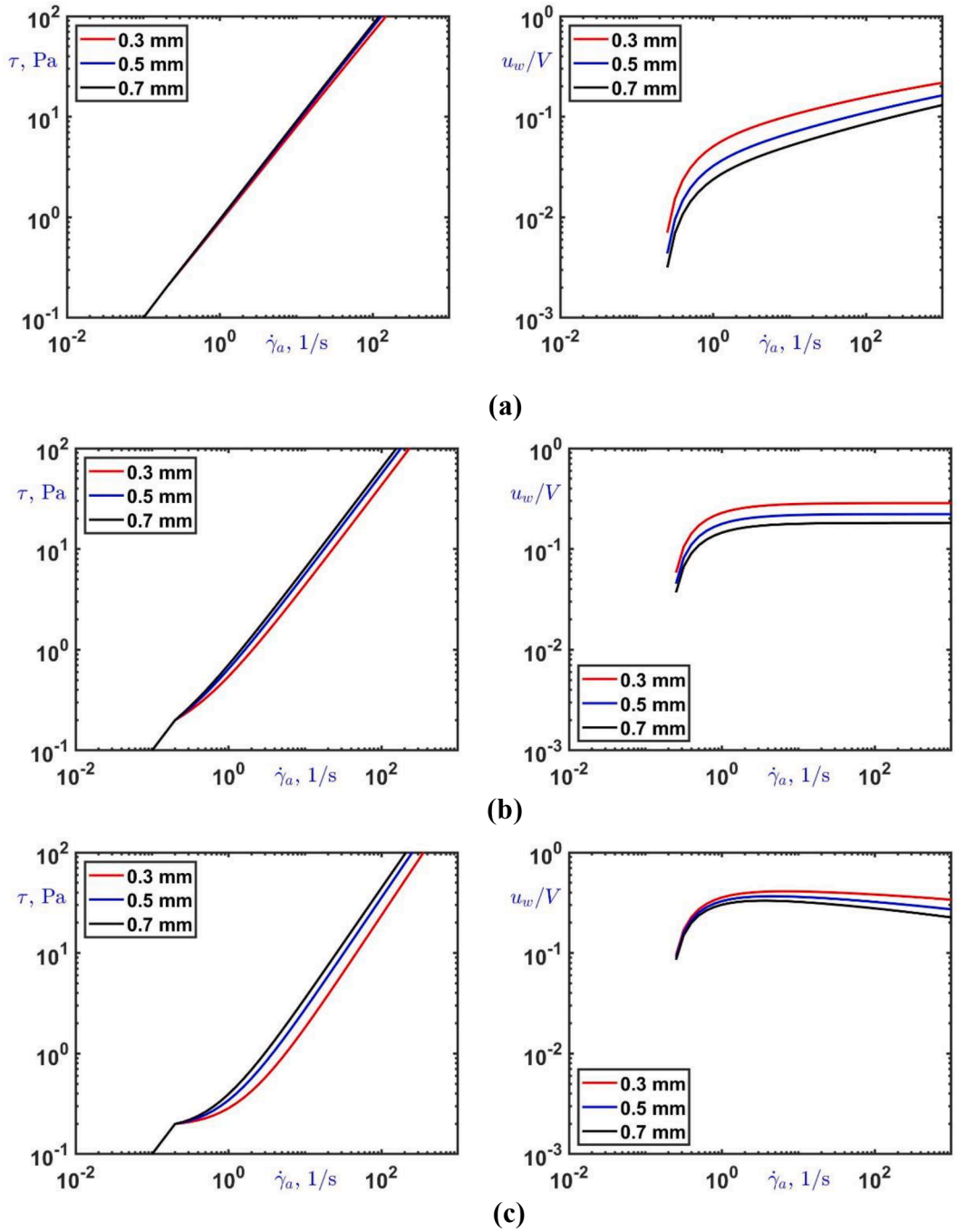

Fig. 6. Flow curves (left) and slip velocities (right) of Newtonian fluids exhibiting slip with $\tau_c = 0.2$Pa (finite slip yield stress), $\beta = 5000\text{Pa}\cdot\text{s}^{1/s}/\text{m}^{1/s}$, and $\mu = 1\text{Pa}\cdot\text{s}$: (a) $s = 0.8$; (b) $s = 1$ (Navier slip); (c) $s = 1.2$.

Thus, the apparent flow curve is described by

$$\tau_w = \begin{cases} k\dot{\gamma}_a^n, & \dot{\gamma}_a \le \dot{\gamma}_{ac} \\ k(1-2u_w/V)^n \dot{\gamma}_a^n, & \dot{\gamma}_a > \dot{\gamma}_{ac} \end{cases} \tag{14}$$

3.1. Newtonian fluids

In Newtonian fluids, the critical apparent shear rate for the occurrence of wall slip is $\dot{\gamma}_{ac} = \tau_c/\mu$. The analytical solutions for $s = 1$ and 2 are easily derived. When $s = 1$, one finds from Eq. (13) that

$$\frac{u_w}{V} = \frac{B\left(1 - \dot{\gamma}_{ac}\Big/\dot{\gamma}_a\right)}{1+2B} \tag{15}$$

where $B \equiv \mu/(\beta H)$ is the dimensionless slip number. The relative slip velocity is bounded above by 1/2, which corresponds to full (ideal) slip. When the slip yield stress is zero, i.e. when we have Navier slip ($\tau_c = 0$ and thus $\dot{\gamma}_{ac} = 0$), the relative velocity is constant (independent of the apparent shear rate). This decreases with the gap size H. If the slip-yield stress is non-zero, the relative slip velocity increases with the apparent shear rate $\dot{\gamma}_a$ and this increase becomes more important as the gap size is reduced.

The apparent flow curve for $n = s = 1$ is given by

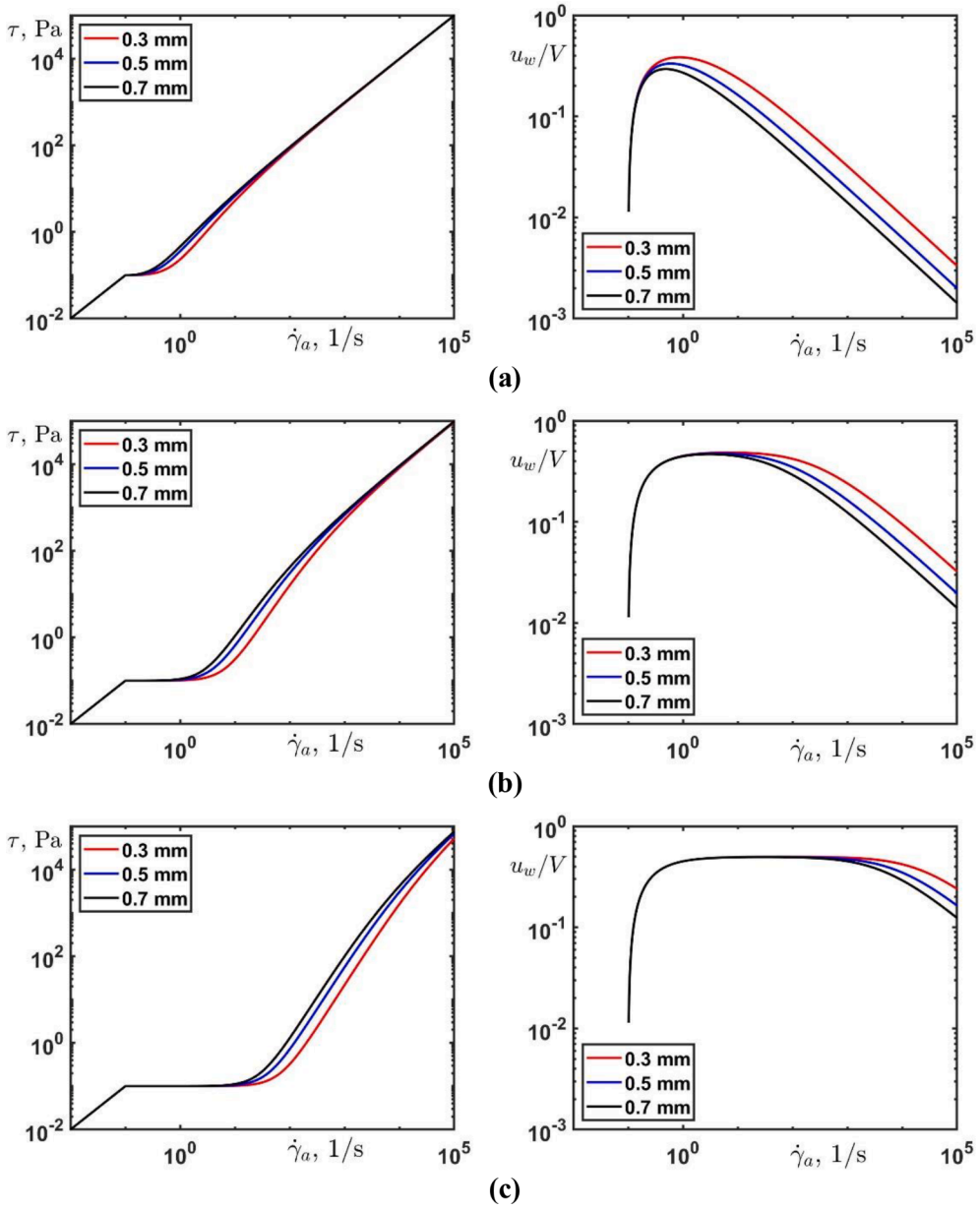

Fig. 7. Effect of the slip coefficient β on the flow curve and the relative slip velocity in the case of Newtonian flow with $\mu = 1$Pa·s, and slip with non-zero slip yield stress ($s = 2$, $\tau_c = 0.1$ Pa): (a) $\beta = 10^7$Pa·s$^{1/s}$/m$^{1/s}$ (weak slip); (b) $\beta = 10^5$Pa·s$^{1/s}$/m$^{1/s}$ (moderate slip); $\beta = 10^3$Pa·s$^{1/s}$/m$^{1/s}$ (strong slip).

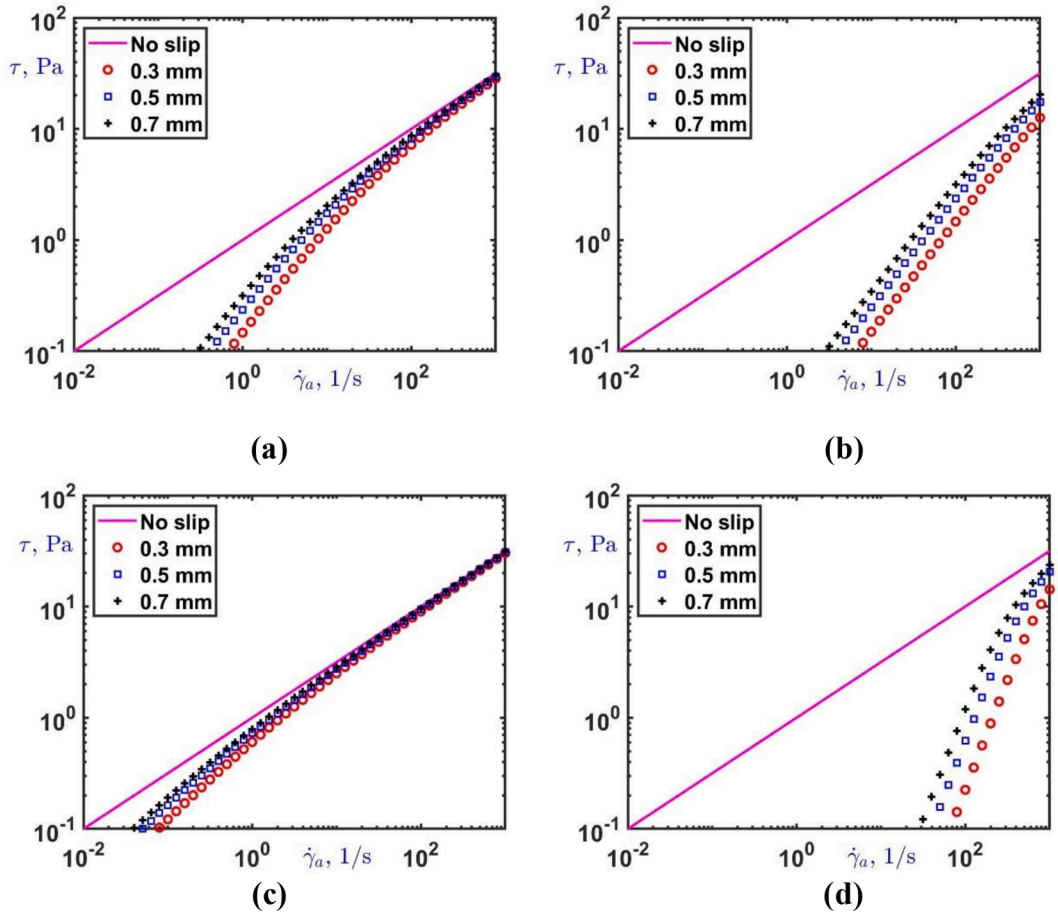

Fig. 8. Apparent flow curves obtained for a power-law fluid ($n = 0.5$ and $k = 1\text{Pa}\cdot\text{s}^{1/2}$) and wall slip with zero slip yield stress ($\tau_c = 0$): (a) $\beta = 1000\text{Pa}\cdot\text{s}/\text{m}$ and $s = 1$ (strong Navier slip); (b) $\beta = 100\text{Pa}\cdot\text{s}/\text{m}$ and $s = 1$ (very strong Navier slip); (c) $\beta = 1000\text{Pa}\cdot\text{s}^{1/s}/\text{m}^{1/s}$ and $s = 0.8$; (d) $\beta = 1000\text{Pa}\cdot\text{s}^{1/s}/\text{m}^{1/s}$ and $s = 1.2$. The flow curve corresponding to no-slip is also shown.

$$\tau_w = \begin{cases} \mu\dot{\gamma}_a, & \dot{\gamma}_a \le \dot{\gamma}_{ac} \\ \dfrac{\mu\left(\dot{\gamma}_a + 2B\dot{\gamma}_{ac}\right)}{1+2B}, & \dot{\gamma}_a > \dot{\gamma}_{ac} \end{cases} \tag{16}$$

The effect of wall slip on the flow curve of a Newtonian fluid is illustrated in Fig. 2. When the slip yield stress is zero, e.g. when Navier slip is applied, $\dot{\gamma}_{ac} = 0$ and slip occurs for any apparent shear rate. The slope of the flow curve is reduced from μ to $\mu/(1+2B)$. If the slip yield stress is finite, the first branch of the flow curve up to $\dot{\gamma}_{ac} = \tau_c/\mu$ coincides with the no-slip flow curve and the second branch is of the same slope as the Navier-slip flow curve.

For $s = 2$, the solution of Eq. (13) is

$$\frac{u_w}{V} = \frac{\sqrt{1+\frac{\beta H^2}{\mu}\left(\dot{\gamma}_a - \dot{\gamma}_{ac}\right)} - 1}{\frac{\beta H^2}{\mu}\dot{\gamma}_a} = \frac{1 - \dot{\gamma}_{ac}\Big/\dot{\gamma}_a}{1+\sqrt{1+\frac{\beta H^2}{\mu}\left(\dot{\gamma}_a - \dot{\gamma}_{ac}\right)}} \tag{17}$$

When the slip yield stress is zero (power-law slip equation with $\tau_c = 0$, the relative velocity is given by

$$\frac{u_w}{V} = \frac{\sqrt{1+\beta H^2\dot{\gamma}_a\Big/\mu} - 1}{\beta H^2\dot{\gamma}_a\Big/\mu} \tag{18}$$

As the apparent shear rate tends to zero, the relative velocity tends to 1/2 (full slip). In the presence of non-zero slip yield stress, when $\dot{\gamma}_a \to \dot{\gamma}_{ac}$, $u_w/V \to 0$. At high values of the apparent shear rate $\dot{\gamma}_a$, the slip velocity may be approximated by

$$\frac{u_w}{V} \simeq \frac{\sqrt{\mu/\beta}}{H\sqrt{\dot{\gamma}_a}} \tag{19}$$

Therefore, u_w/V is a decreasing function at high values of the apparent shear rate. Given that u_w/V is increasing initially (when the slip yield stress is non-zero, $\tau_c > 0$), a global maximum appears at a critical shear rate. Taking the Taylor expansion of the nominator of Eq. (17) yields

$$\frac{u_w}{V} \simeq \frac{1}{2}\left(1 - \frac{\dot{\gamma}_{ac}}{\dot{\gamma}_a}\right)\left[1 - \frac{1}{4}\frac{\beta H^2}{\mu}\left(\dot{\gamma}_a - \dot{\gamma}_{ac}\right)\right] \tag{20}$$

It is straightforward to show that the maximum of the slip velocity is at

$$\dot{\gamma}_a^* = \sqrt{\left(\frac{4\mu}{\beta H^2} + \dot{\gamma}_{ac}\right)\dot{\gamma}_{ac}} \tag{21}$$

Clearly, the maximum moves to the right as τ_c is increased, or as slip is enhanced (β is reduced).

The flow curve when $s = 2$ is described by

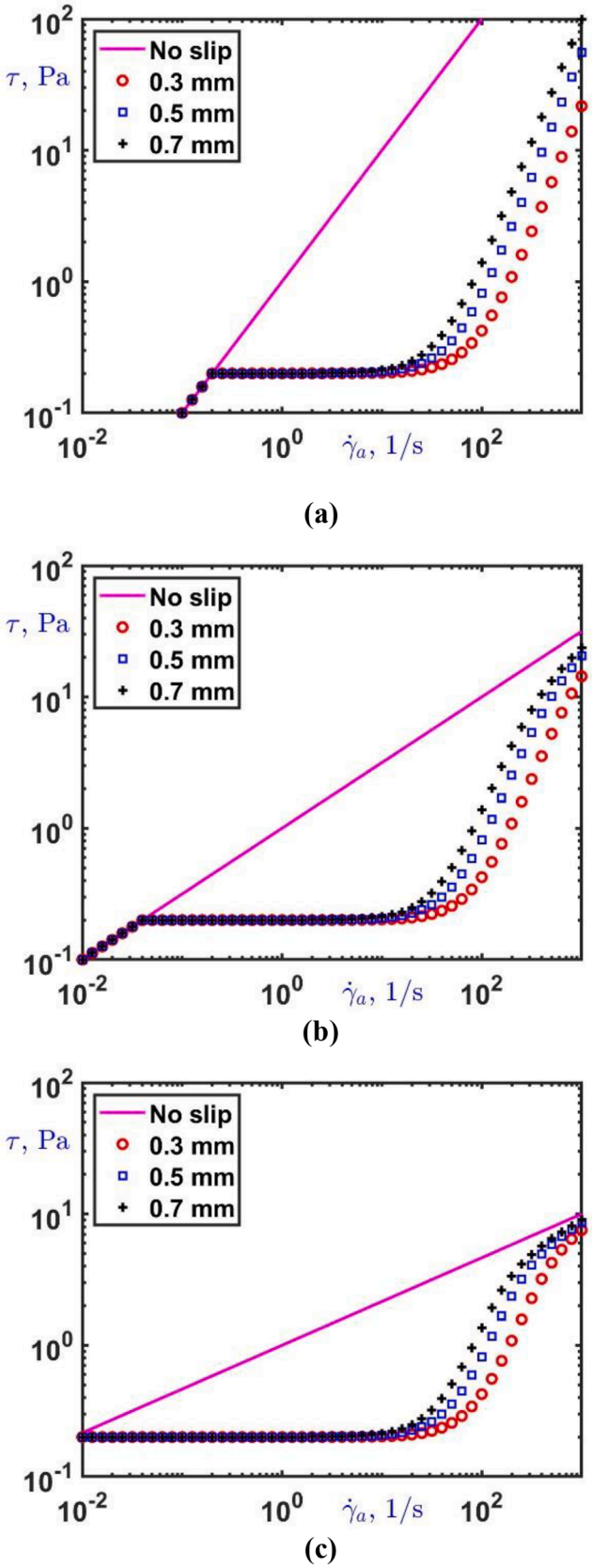

Fig. 9. Flow curves of power-law fluids with $k = 1\text{Pa}\cdot\text{s}^n$, $\tau_c = 0.2\text{Pa}$, $\beta = 1000\text{Pa}\cdot\text{s}^{1/s}/\text{m}^{1/s}$ and $s = 2$: (a) $n = 1$; (b) $n = 0.5$; (c) $n = 1/3$. The straight line is the flow curve corresponding to no-slip.

$$\tau_w = \begin{cases} \mu\dot{\gamma}_a, & \dot{\gamma}_a \le \dot{\gamma}_{ac} \\ \mu\left\{\dot{\gamma}_a - \dfrac{2\mu}{\beta H^2}\left[\sqrt{1+\dfrac{\beta H^2}{\mu}\left(\dot{\gamma}_a - \dot{\gamma}_{ac}\right)} - 1\right]\right\}, & \dot{\gamma}_a > \dot{\gamma}_{ac} \end{cases} \tag{22}$$

When $\tau_c = 0$ and the apparent shear rate is high,

$$\tau_w \approx \frac{\mu^2}{\beta H^2}\frac{\beta H^2}{\mu}\dot{\gamma}_a = \mu\dot{\gamma}_a \tag{23}$$

and, therefore, the flow curve tends asymptotically to its no-slip counterpart. From Eq. (22), we can deduce that $\tau \approx \tau_c$ for small values of the apparent shear rate, $\tau \approx \tau_c$ and that for high values of the apparent shear rate, $\tau \to \mu\dot{\gamma}_a$. For moderate values of the apparent shear rate we get:

$$\tau_w \approx \tau_c + \frac{1}{4}\beta H^2\left(\dot{\gamma}_a - \dot{\gamma}_c\right)^2 \tag{24}$$

In is clear that in this intermediate regime the effect of the gap size becomes important. Eq. (24) predicts that the shear stress grows faster as the gap size is increased or as slip becomes weaker.

To visualize the gap-size effects, we obtained results for three different values of the gap size: $H = 0.3\text{mm}, 0.5\text{mm}, \text{and}0.7\text{mm}$. Let us start with the zero-slip-yield-stress case, in which the no-slip branch does not exist. In Fig. 3, the apparent flow curves (plots of τ versus the apparent shear rate $\dot{\gamma}_a$) for $\mu = 1\text{Pa}\cdot\text{s}$ and different values of the slip coefficient and the slip exponent are shown together with the no-slip flow curve, for the sake of comparison. As expected, wall slip shifts the flow curve to the right (the required shear stress for a given value of $\dot{\gamma}_a$ decreases as the slip coefficient is reduced) and this effect is enhanced as the gap size is reduced. In the case of Navier slip ($s = 1$), the flow curves are straight lines the slopes of which are independent of the gap size and decrease as slip becomes stronger (as B is increased; see Eq. (16)). The effect of the slip exponent is also important. It is interesting to note that the flow curves corresponding to different gap sizes tend to diverge when $s < 1$ (Fig. 3c) and to merge when $s > 1$ (Fig. 3d). Hence, the material appears to slightly shear-thicken when $s > 1$ and shear-thin when $s < 1$.

The effect of the slip yield stress is illustrated in Fig. 4, where we show results obtained with $\tau_c = 0.2\text{Pa}$, $\beta = 1000\text{Pa}\cdot\text{s}^{1/s}/\text{m}^{1/s}$ and different values of the viscosity and the slip exponent. The flow curves initially coincide with their no-slip counterpart, then exhibit a plateau corresponding to the slip yield stress τ_c, and eventually approach asymptotically their zero-τ_c counterparts. They thus appear to diverge when $s < 1$ and to merge when $s > 1$. It seems that the shear stress plateau is enhanced as the viscosity is increased and/or slip becomes stronger, i.e. when s is increased or β is reduced (Fig. 4d).

The variation of the relative slip velocity u_w/V with the apparent shear rate is illustrated in Figs. 5 and 6 for $\tau_c = 0$ and $\tau_c = 0.2\text{Pa}$, respectively. In Fig. 5, the flow curves for the latter case with $\mu = 1\text{Pa}\cdot\text{s}$, $\beta = 5000\text{Pa}\cdot\text{s}^{1/s}/\text{m}^{1/s}$ and various values of the slip exponent are plotted together with the corresponding slip velocities. As already mentioned, the slip velocity decreases with the gap size and is independent of the apparent shear rate in the case of Navier slip ($s = 1$). When $s < 1$, u_w/V increases with $\dot{\gamma}_a$ and tends to reach asymptotically the corresponding Navier-slip value. When $s > 1$, u_w/V is initially equal to the limiting value 1/2 and decreases with $\dot{\gamma}_a$.

More interesting are the results for non-zero slip yield stress in Fig. 6. Since the slip velocity is zero for $\dot{\gamma}_a \le \dot{\gamma}_{ac}$, it increases rapidly approaching asymptotically its zero-τ_c counterpart (shown in Fig. 5). Thus, the slip velocity is an increasing function of the apparent shear rate when $s \le 1$, levelling to a constant value when $s = 1$ (Navier slip). When $s > 1$, however, u_w is increasing initially and decreasing at higher shear rates, thus passing through a global maximum. The approximate location of the maximum when $s = 2$ is given by Eq. (21). The effect of the slip coefficient for $s = 2$ and $\tau_c = 0.1\text{Pa}$ is illustrated in Fig. 7. As

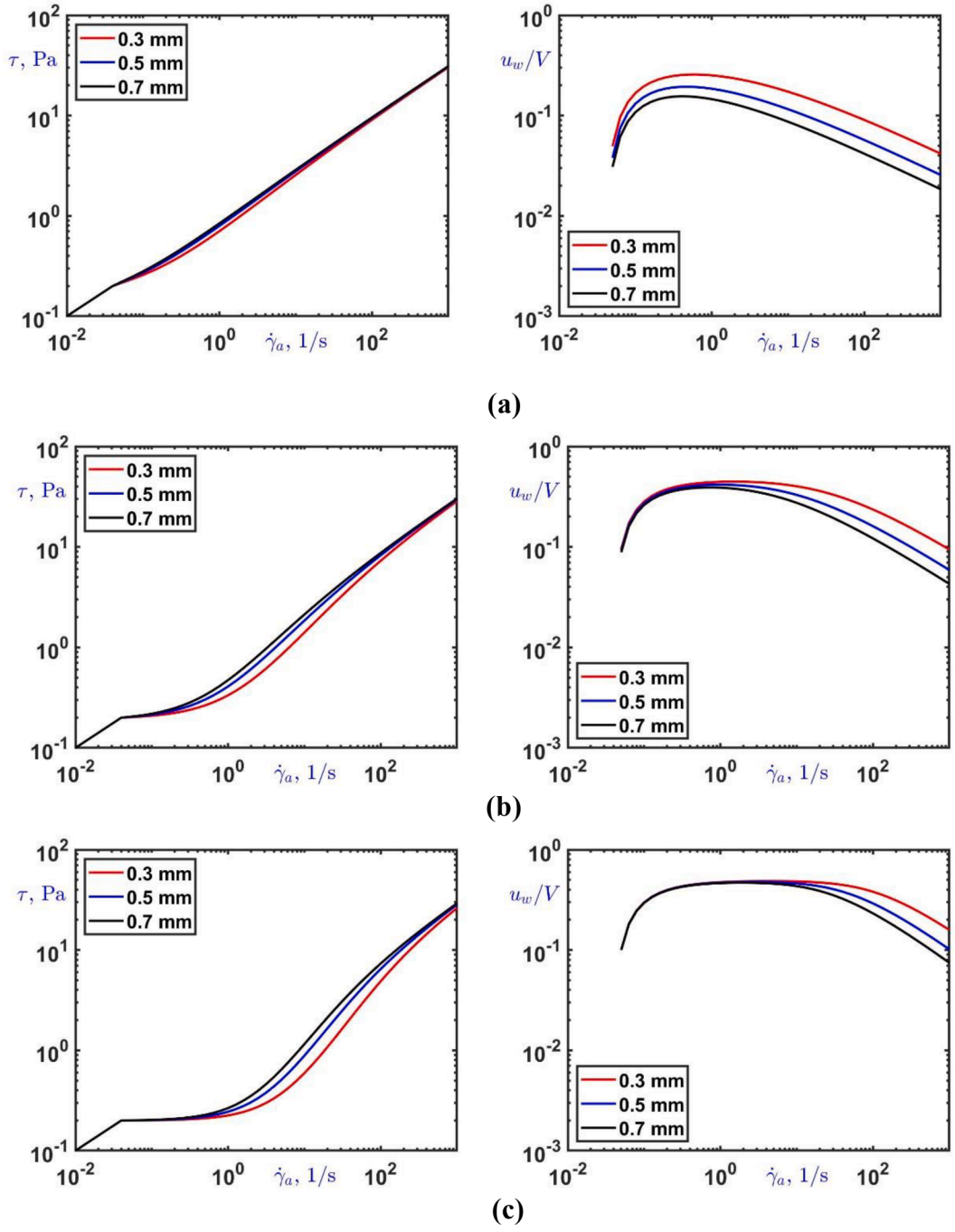

Fig. 10. Flow curves (left) and slip velocities (right) of a power-law fluid with $n = 1/2$ and $k = 1\text{Pa}\cdot\text{s}^{1/2}$, $\tau_c = 0.2\text{Pa}$ and $\beta = 5000\text{Pa}\cdot\text{s}^{1/s}/\text{m}^{1/s}$: (a) $s = 0.8$; (b) $s = 1$ (Navier slip); (c) $s = 1.2$.

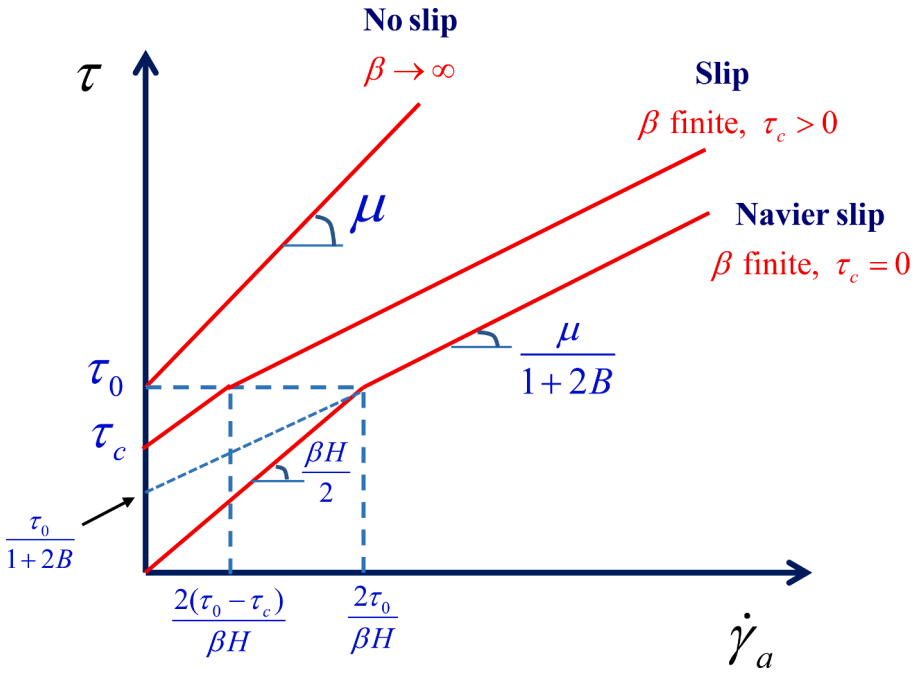

Fig. 11. Apparent flow curves of a Bingham plastic with no-slip, Navier slip, and slip with non-zero slip yield stress. In the case of slip, the flow curve consists of the sliding and the yielding branches below and above the critical apparent shear rate $\dot{\gamma}_{a0} = 2(\tau_0 - \tau_c)/(\beta H)$. The sliding branch has a slope of $\beta H/2$ and ranges from τ_c to τ_0; hence, if Navier slip applies ($\tau_c = 0$), this ranges from 0 to τ_0.

dictated by Eq. (21), the slip velocity maximum moves to the right as slip becomes stronger, as predicted by Eq. (21).

3.2. Power-law fluids

When $n = 1/2$ and $\dot{\gamma}_a \le \dot{\gamma}_{ac} = (\tau_c/k)^2$, no slip occurs and the apparent flow curve coincides with the true one, $\tau_w = k\sqrt{\dot{\gamma}_a}$. In the slip regime ($\dot{\gamma}_a > \dot{\gamma}_{ac}$), one obtains the following expression for the slip velocity:

$$\frac{u_w}{V} = \frac{k^2}{\beta^2 H^2 \dot{\gamma}_a}\left[\sqrt{1+\frac{2\beta H}{k}\sqrt{\dot{\gamma}_{ac}}+\frac{\beta^2 H^2}{k^2}\dot{\gamma}_a}-\left(1+\frac{\beta H}{k}\sqrt{\dot{\gamma}_{ac}}\right)\right] \tag{25}$$

The apparent flow curve is given by

$$\tau_w = \begin{cases} \mu\sqrt{\dot{\gamma}_a}, \dot{\gamma}_a \le \dot{\gamma}_{ac} \\ \mu\left\{\dot{\gamma}_a - \frac{2k^2}{\beta^2 H^2}\left[\sqrt{1+\frac{2\beta H}{k}\sqrt{\dot{\gamma}_{ac}}+\frac{\beta^2 H^2}{k^2}\dot{\gamma}_a}-\left(1+\frac{\beta H}{k}\sqrt{\dot{\gamma}_{ac}}\right)\right]\right\}^{1/2}, \dot{\gamma}_a > \dot{\gamma}_{ac} \end{cases} \tag{26}$$

Fig. 8 illustrates the effects of the slip parameters on the flow curves of a shear-thinning fluid ($n = 0.5$ and $k = 1\text{Pa}\cdot\text{s}^{1/2}$) with zero slip yield stress ($\tau_c = 0$). As with Newtonian fluids, stronger wall slip (which is equivalent to smaller β and/or bigger s) shifts the flow curve to the right and this effect is more visible when the gap between the plates is reduced. Due to slip the flow curves are below their no-slip counterpart, and the deviations are larger at low apparent shear rates, due to shear thinning.

The effects of the exponents n and s are illustrated in Figs. 9 and 10, respectively. In Fig. 9, results obtained with $k = 1\text{Pa}\cdot\text{s}^n$, $\tau_c = 0.2\text{Pa}$, $\beta = 1000\text{Pa}\cdot\text{s}^{1/s}/\text{m}^{1/s}$, and $s = 2$ are shown. As dictated by Eq. (12), the critical apparent shear rate $\dot{\gamma}_{ac}$ at which slip occurs is reduced and the size of the plateau region is increased with shear thinning. As with Newtonian fluids, the gap-dependence of the apparent flow curve is enhanced by slip, e.g. with the slip exponent s. We observe in Fig. 10, that the lower the value of s the sharper the slip velocity maximum.

4. Results for Herschel-Bulkley fluids

We first present analytical solutions for the Bingham plastic ($n = 1$). When $s = 1$, Eq. (8) yields the following expression for the critical apparent shear rate for yielding

$$\dot{\gamma}_{a0} = \frac{2(\tau_0 - \tau_c)}{\beta H} \tag{27}$$

From Eqs. (10) and (11), we find that

$$\frac{u_w}{V} = \frac{2B + \dot{\gamma}_{a0}/\dot{\gamma}_a}{2(1+2B)}, \quad \dot{\gamma}_a > \dot{\gamma}_{a0} \tag{28}$$

and

$$\tau_w = \begin{cases} \tau_c + \beta H \dot{\gamma}_a/2, & \dot{\gamma}_a \le \dot{\gamma}_{a0} \\ \tau_0 + \frac{\mu\left(\dot{\gamma}_a - \dot{\gamma}_{a0}\right)}{1+2B}, & \dot{\gamma}_a > \dot{\gamma}_{a0} \end{cases} \tag{29}$$

The effects of slip on the apparent flow curve of a Bingham plastic are illustrated in Fig. 11. In the absence of slip, the material is yielded for all values of the apparent shear rate and the flow curve is a straight line of slope μ with $\tau_w \ge \tau_0$. When slip does occur, the flow curve consists of two branches corresponding to the sliding and yielding regimes. If $\tau_c = 0$, i.e. if Navier slip applies, the first branch up to the critical apparent shear rate $\dot{\gamma}_{a0} = 2\tau_0/(\beta H)$ with $0 \le \tau_w \le \tau_0$ is of slope $\beta H/2$. The second branch where $\tau_w > \tau_0$ is of slope $\mu/(1+2B)$. In a log-log plot the flow curve is characterized by an intermediate plateau corresponding to the yield stress, as, for example, in Fig. 12a. If the slip yield stress is finite ($\tau_c > 0$), the flow curve is shifted to the left so that the sliding branch

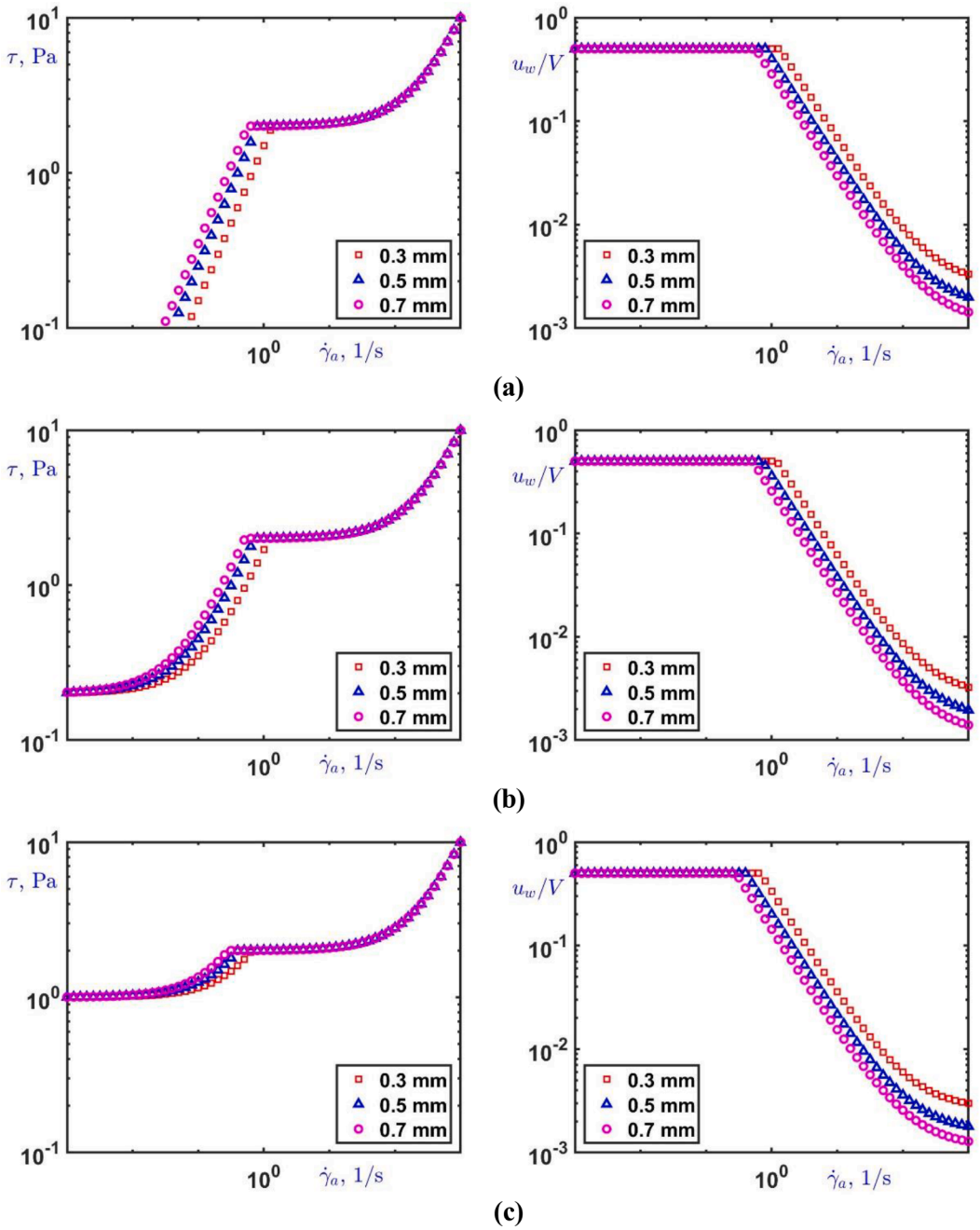

Fig. 12. Effect of the slip yield stress on the flow curve and the relative slip velocity in the case of Herschel-Bulkley fluid with $\tau_0 = 2$Pa, $s = 1$, $\beta = 1{\cdot}10^4$Pa·s^s /m^s, $n = 1$ and $k = 8{\cdot}10^{-3}$Pa·s^n: (a) $\tau_c = 0$; (b) $\tau_c = 0.2$Pa; (c) $\tau_c = 1$Pa.

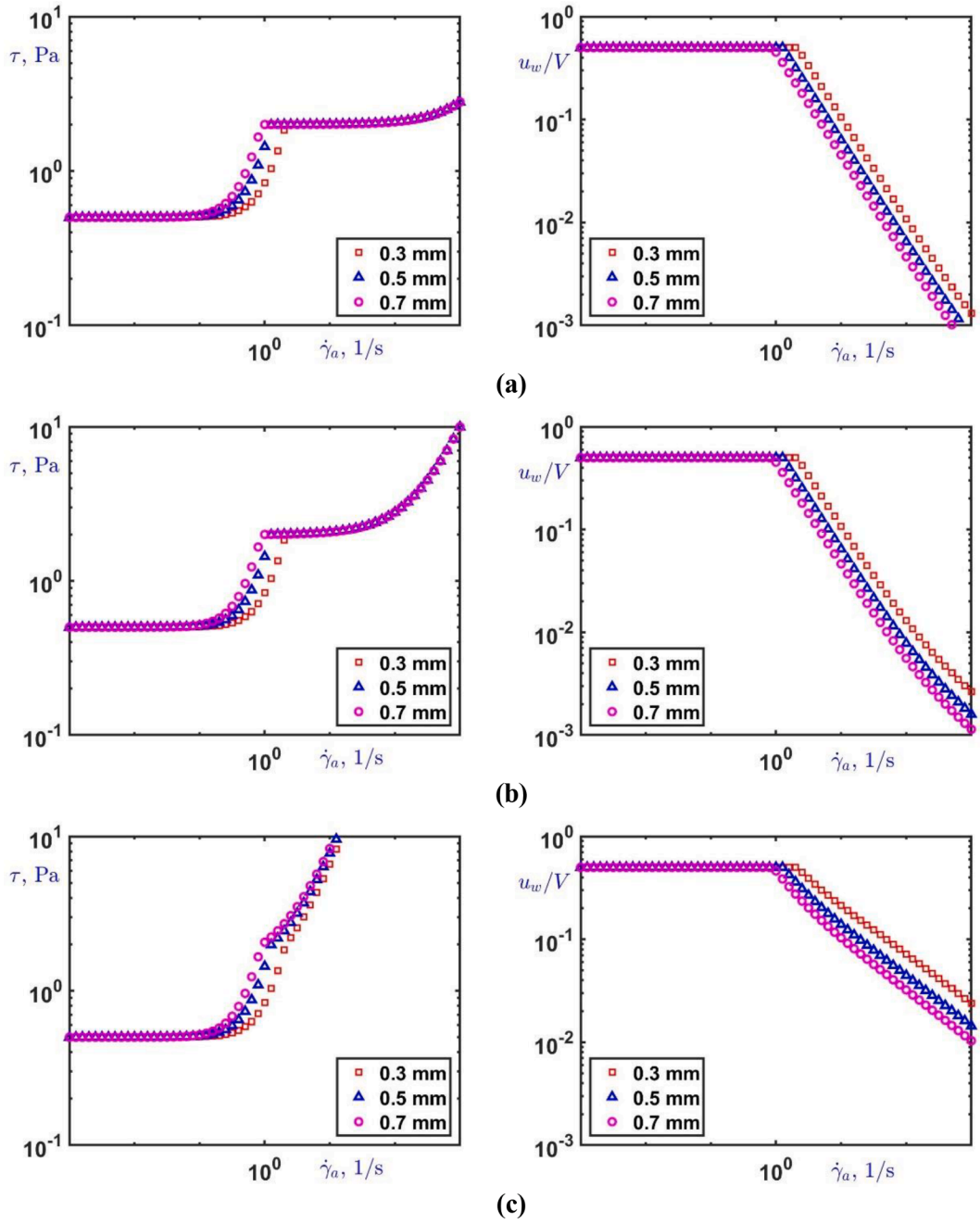

Fig. 13. Effect of the consistency index on the flow curve and the relative slip velocity in the case of Herschel-Bulkley fluid with $\tau_c = 0.5$Pa, $\tau_0 = 2$Pa, $s = 2$, $\beta = 1.5{\cdot}10^7$Pa·s^s/m^s, and $n = 1$: (a) $k = 8{\cdot}10^{-4}$Pa·s; (b) $k = 8{\cdot}10^{-3}$Pa·s; (c) $k = 8{\cdot}10^{-1}$Pa·s.

extends up to $\dot{\gamma}_{a0} = 2(\tau_0 - \tau_c)/(\beta H)$ and $\tau_c \le \tau_w \le \tau_0$. Hence, the apparent (log-log) flow curve is characterized by two plateaus corresponding to the slip yield stress and the yield stress, as in Fig. 12.

In the case of a Bingham plastic exhibiting slip with $s = 2$, one finds that

$$\dot{\gamma}_{a0} = \frac{2}{H}\sqrt{\frac{\tau_0 - \tau_c}{\beta}} \tag{30}$$

$$\frac{u_w}{V} = \frac{1}{\dot{\gamma}_a}\left[\sqrt{\frac{\dot{\gamma}_{a0}^2}{4} + \left(\frac{\mu}{\beta H^2} + \dot{\gamma}_a\right)\frac{\mu}{\beta H^2}} - \frac{\mu}{\beta H^2}\right], \quad \dot{\gamma}_a > \dot{\gamma}_{a0} \tag{31}$$

and

$$\tau_w = \begin{cases} \tau_c + \beta H^2 \dot{\gamma}_a^2/4, & \dot{\gamma}_a \le \dot{\gamma}_{a0} \\ \tau_0 + \mu\left\{\dot{\gamma}_a - 2\left[\sqrt{\frac{\dot{\gamma}_{a0}^2}{4} + \left(\frac{\mu}{\beta H^2} + \dot{\gamma}_a\right)\frac{\mu}{\beta H^2}} - \frac{\mu}{\beta H^2}\right]\right\}, & \dot{\gamma}_a > \dot{\gamma}_{a0} \end{cases} \tag{32}$$

For a Herschel-Bulkley fluid with $n = 1/2$ and $s = 1$, the critical apparent shear rate $\dot{\gamma}_{a0}$ is given by Eq. (27). For the slip velocity and the apparent flow curve one gets:

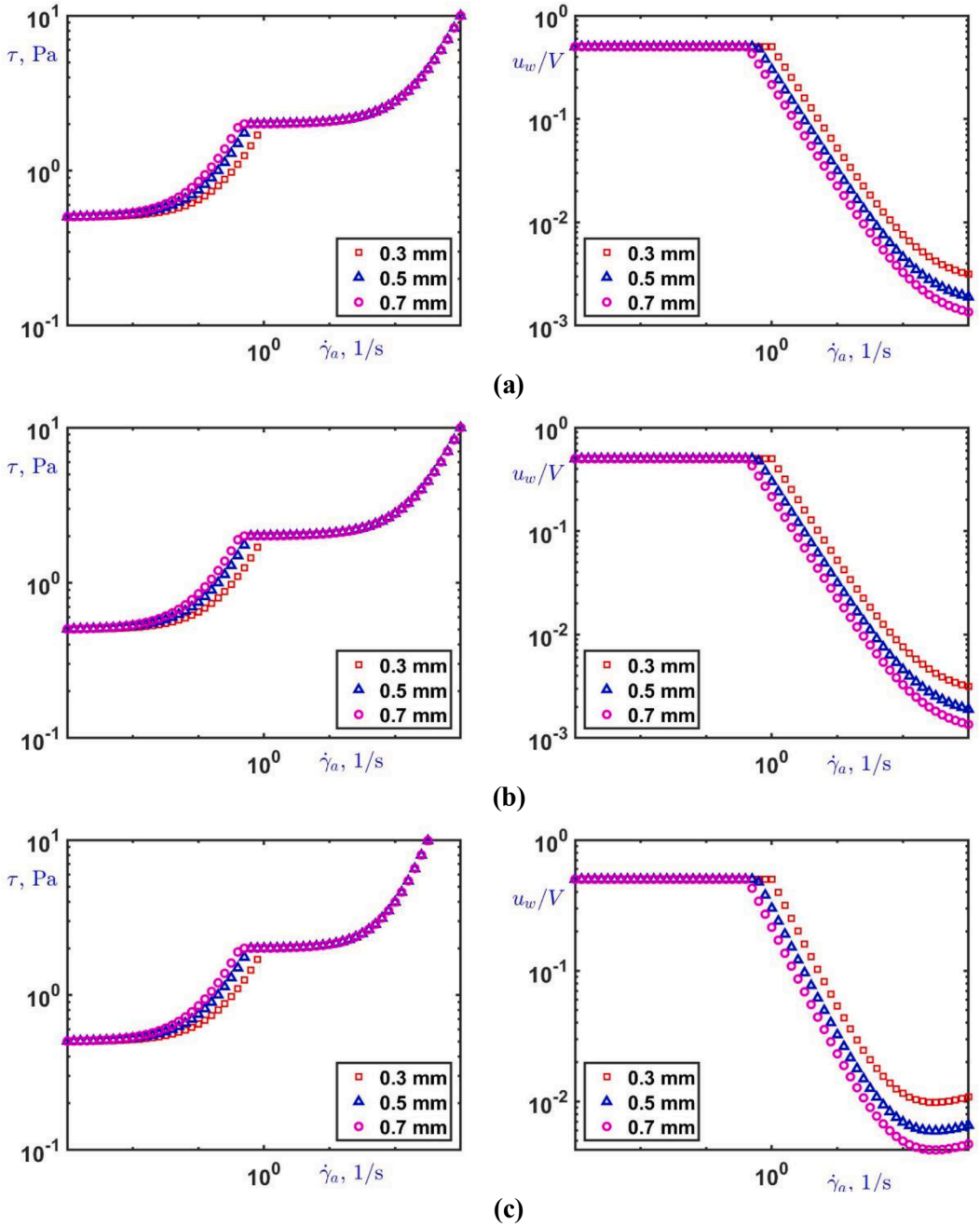

Fig. 14. Effect of the power-law exponent on the flow curve and the relative slip velocity in the case of Herschel-Bulkley fluid with $\tau_c = 0.5$Pa, $\tau_0 = 2$Pa, $s = 1$, $\beta = 1{\cdot}10^4$Pa$\cdot$s^s/m^s, and $k = 8{\cdot}10^{-3}$Pa$\cdot$s^n: (a) $n = 0.8$ (shear thinning); (b) $n = 1$ (Bingham plastic); (c) $n = 1.2$ (shear thickening).

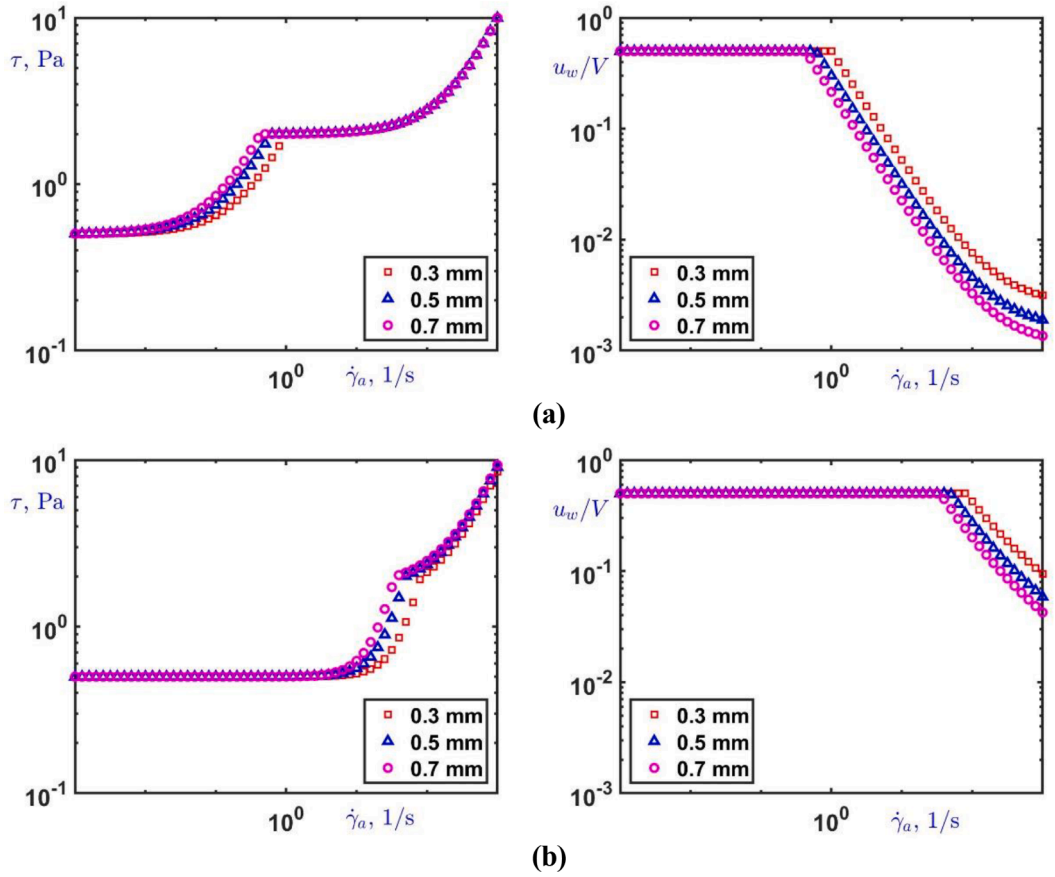

Fig. 15. Effect of the slip exponent on the flow curve and the relative slip velocity in the case of Herschel-Bulkley fluid with $\tau_c = 0.5$Pa, $\tau_0 = 2$Pa, $\beta = 1{\cdot}10^4$Pa·s^s/m^s, $n = 1$ and $k = 8{\cdot}10^{-3}$Pa·s^n: (a) $s = 1$; (b) $s = 2$.

$$\frac{u_w}{V} = \frac{1}{2}\left[1 - \frac{1}{\dot{\gamma}_a}\left(\sqrt{\frac{k^2}{\beta^2 H^2} + \frac{\dot{\gamma}_a - \dot{\gamma}_{a0}}{2}} - \frac{k}{\beta H}\right)^2\right], \quad \dot{\gamma}_a > \dot{\gamma}_{a0} \tag{33}$$

and

$$\tau_w = \begin{cases} \tau_c + \beta H \dot{\gamma}_a/2, & \dot{\gamma}_a \le \dot{\gamma}_{a0} \\ \tau_0 + k\left(\sqrt{\frac{k^2}{\beta^2 H^2} + \frac{\dot{\gamma}_a - \dot{\gamma}_{a0}}{2}} - \frac{k}{\beta H}\right), & \dot{\gamma}_a > \dot{\gamma}_{a0} \end{cases} \tag{34}$$

For the discussion of the results, we use the following 'base values' for the various parameters: $\tau_c = 0.5$Pa, $\tau_0 = 2$Pa, $s = 1$, $\beta = 1{\cdot}10^4$Pa·s^s/m^s, $n = 1$, and $k = 8{\cdot}10^{-3}$Pa·s^n. These have been selected so that the two critical stresses, τ_c and τ_0, and the critical shear rate $\dot{\gamma}_{ac}$ are close to the critical values deduced from the experiments on a 8%vol suspension of kaolinite (Moud et al., 2021a). In Figs. 12–17, we show the flow curves (left column) and the dimensionless slip velocity u_w/V (right column).

The effect of the slip yield stress is illustrated in Fig. 12, where results for $\tau_c = 0$, 0.2 and 1 Pa are shown. As expected, the gap-size effect on the left branch of the flow curve (Regime 1) becomes more pronounced as the difference $\tau_0 - \tau_c$ increases. Due to fact that the slip-yield-stress in Fig. 12a is zero, the flow curve exhibits only the yield-stress plateau. Clearly, yield stress materials with apparent flow curves with only one stress plateau slip with zero slip yield stress. This is the case, for example, with the parallel-plate experiments of Seth et al. (2008) on microgel pastes, the sliding-plate data of Jofore et al. (2015) on a Carbopol microgel, and the data of Clasen (2012) on an aqueous xanthan gum solution determined with cone-and-plate and sliding-plate rheometers.

The flow curves with a finite slip yield stress consist of two branches corresponding to Regimes 1 and 2 described in Section 2. Initially the flow curve is flat and then becomes increasing till the critical shear rate $\dot{\gamma}_{ac}$ is reached. It is in this region (the last part of Regime 1) where the gap-size effect is enhanced. Note also that $\dot{\gamma}_{ac}$ increases as H is reduced. Just above $\dot{\gamma}_{ac}$, i.e. in Regime 2, the flow curve becomes flat again and then starts increasing, as in the parallel disk data of Ewoldt et al. (2015) on a Nivea Lotion for different gap heights. These authors noted that the existence of the apparent stress plateau at low shear rates, which is equivalent to an 'apparent dynamic yield stress', is a common experimental artifact for yield stress fluids, such as dense colloidal systems.

The dimensionless slip velocities are shown in the right column of Fig. 12. The relative velocity u_w/V is constant in the sliding regime and starts decreasing in the yielding regime, i.e. when $\dot{\gamma}_{ac}$ is exceeded. As expected, changing the slip yield stress has no effect on the relative slip velocity in both Regimes 1 and 2.

As illustrated in Fig. 13, where results for $k = 8{\cdot}10^{-4}$Pa·s, $8{\cdot}10^{-3}$Pa·s and $8{\cdot}10^{-1}$Pa·s are plotted, the consistency index has no effect on the branch corresponding to Regime 1. As k is increased, the right branch of the flow curve is shifted to the left and its slope increases. We also observe that slip becomes stronger as the consistency index is increased.

In Fig. 14, where results for different values of the flow index are shown, we notice that the yielding branch of the flow curve is shifted to the left as the exponent n is increased. Moreover, slip is reduced as the flow index is increased. However, as discussed below this may not be the case when the slip exponent $s > 1$.

As deduced from Fig. 15, the effect of the slip exponent s is quite dramatic. As s is increased the value of the critical shear rate $\dot{\gamma}_{ac}$ increases and the gap-size effect is enhanced in both branches of the flow

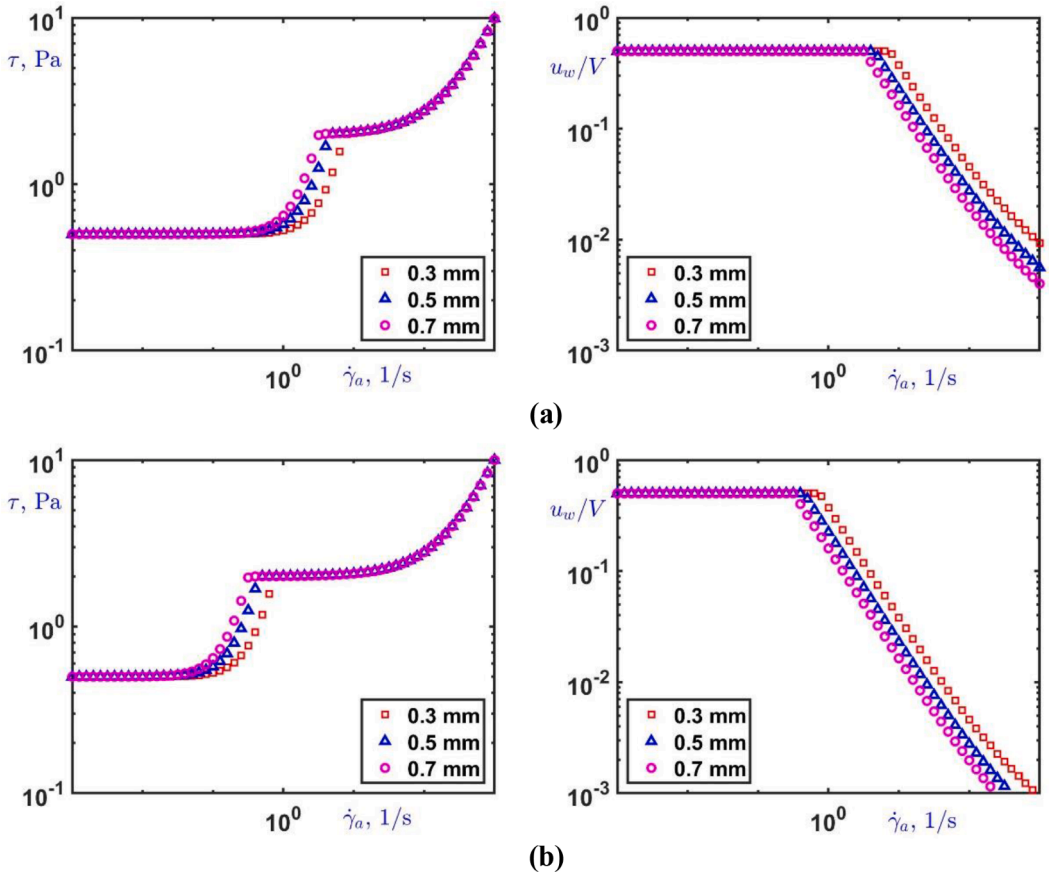

Fig. 16. Effect of slip parameter β on the flow curve and the relative slip velocity in the case of Herschel-Bulkley fluid with $\tau_c = 0.5$Pa, $\tau_0 = 2$Pa, $s = 2$, $n = 1$, and $k = 8{\cdot}10^{-1}$Pa·s: (a) $\beta = 1.2{\cdot}10^{6}$Pa·s^2/m^2; (b) $\beta = 1.2{\cdot}10^{8}$Pa·s^2/m^2.

curve (higher values of s correspond to stronger slip).

It seems that these results are similar to the experiments of Moud et al. (2021a) when $s > 1$. Thus, we switch to $s = 2$ and increase the slip parameter β so that the critical shear rate $\dot{\gamma}_{ac}$ is close to the experimental observations. The effect of β is illustrated in Fig. 16 where results for $\tau_c = 0.5$Pa, $\tau_0 = 2$Pa, $s = 2$, $n = 1$, and $k = 8{\cdot}10^{-3}$Pa·s are shown. As β is increased, slip becomes weaker and the left branch of the flow curve is shifted to the left.

Finally, in Fig. 17, we show results obtained with $\tau_c = 0.5$Pa, $\tau_0 = 2$Pa, $s = 2$, $\beta = 1.5{\cdot}10^{7}$Pa·s^2/m^2, and $k = 0.8$Pa·s^n and $n = 0.5$ and 1. The slope of the yielding branch increases and the gap-size effect becomes more pronounced as shear thinning is reduced. Since $s > 1$, slip is enhanced as n increases.

6. Conclusion

The simple shear flow of Herschel-Bulkley fluids exhibiting slip with non-zero slip yield stress lower than the yield stress has been analyzed. For general values of the flow index n and the slip exponent s, the slip velocity can be calculated numerically. The apparent flow curve, constructed by means of explicit analytical expressions, consists of a sliding and a yielding branch, the first parts of which correspond to stress plateaus between which the flow curve is strongly gap-height dependent. Hence, in the sliding regime, apparent yielding is observed below the actual yield stress of the material, a phenomenon sometimes referred to as 'dynamic yield stress' (Ewoldt et al., 2015). The critical apparent shear rate marking the transition depends on the difference between the slip yield stress and the yields stress, the other slip parameters, such as the slip coefficient and the exponent, and on the gap size. Analytical solutions for the slip velocity and the apparent flow curve have also been derived for certain combinations of the flow index and the slip exponent. It has been demonstrated in particular that apparent shear thinning or shear thickening may be observed if the slip exponent is less or greater than unity.

To illustrate the gap-size effect of wall slip, results for different gap heights, have been obtained. The numerical experiments demonstrated that the sliding branch of the flow curve is initially flat with the shear stress being equal to the slip yield stress τ_c and then starts increasing to reach the yield stress value τ_0. The yielding branch is also quite similar, being initially flat equal to the yield stress τ_0 and then starts increasing. The flow curves corresponding to different gap sizes merge at low and high nominal shear rates, in agreement with experimental data (Ewoldt et al., 2015; Moud et al., 2021a). In other words, gap-size effects are more pronounced in the second part of the sliding regime and occasionally in the early stages of the yielding regime. The slip yield stress and the yield stress can thus directly be determined from the experimental data as the values corresponding to the two plateaux of the flow curve. The critical shear rate $\dot{\gamma}_{a0} = 2[(\tau_0 - \tau_c)/\beta]^{1/s}/H$ can also be determined from the experimental data as the average value of $H\dot{\gamma}_{ac}/2$ calculated for different gap sizes. The values of β and s can be determined from the experimental data in the sliding regime using Eq. (7). Finally, the rheological constants, such as the consistency index and the flow index, can be determined from the experimental data in the yielding regime by means of the constitutive equation.

The next step of the present research is to systematically analyze the flow of viscoplastic materials exhibiting slip with non-zero slip yield stress in a rotational parallel-plate rheometer and make direct comparisons with available experimental data. Such preliminary comparisons have been already made in a recent paper by Moud et al. (2021b) with data on kaolinite suspensions. The experimental data in this paper

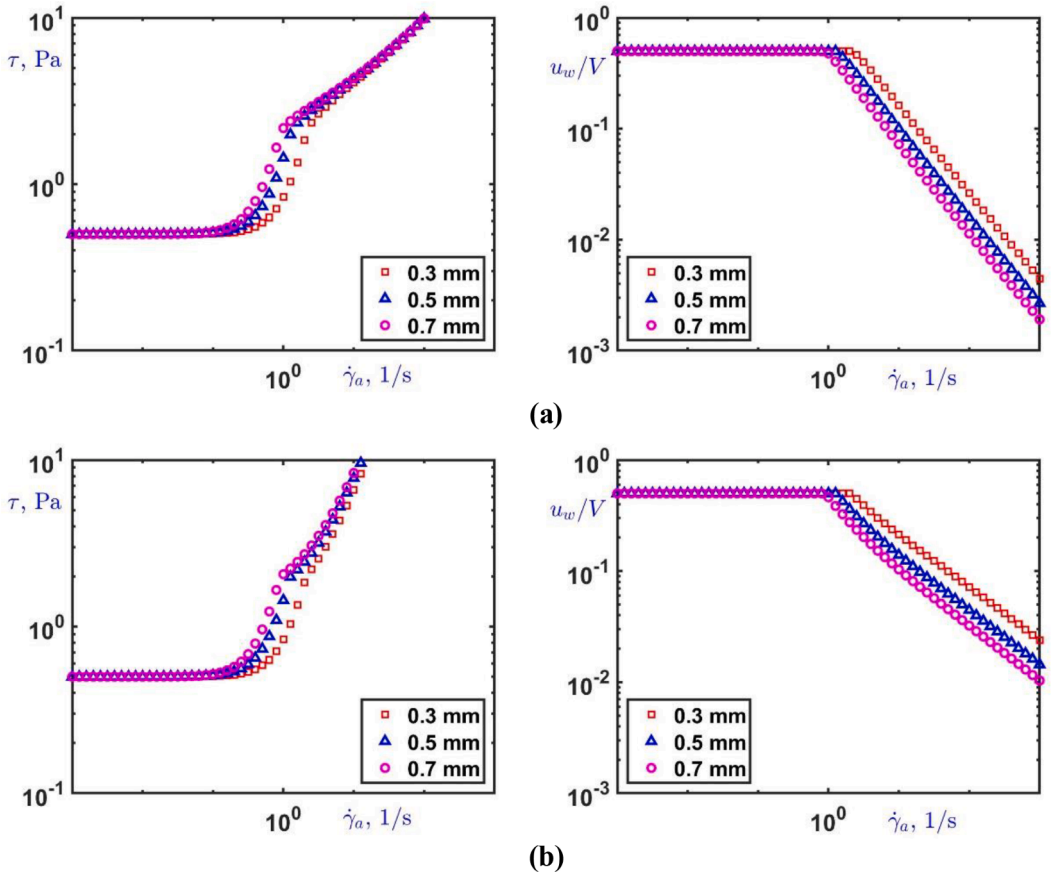

Fig. 17. Effect of the power-law exponent n on the flow curve and the relative slip velocity in the case of Herschel-Bulkley fluid with $\tau_c = 0.5$Pa, $\tau_0 = 2$Pa, $s = 2$, $\beta = 1.5{\cdot}10^7$Pa·s^s/m^s, and $k = 0.8$Pa·s^n: (a) $n = 0.5$; (b) $n = 1$.

revealed that different slip laws apply in the sliding and yielding regimes, a possibility worthy of further investigation both experimentally and theoretically.

Declaration of Competing Interest

The author declares that there is no conflict of interest.

References

Anastasiadis, S., Hatzikiriakos, S.G., 1998. The work of adhesion of polymer/wall interfaces and its association with the onset of wall slip. J. Rheol. 42, 795–812.

Ballesta, P., Besseling, R., Isa, L., Petekidis, G., 2008. Slip and flow of hard-sphere colloidal glasses. Phys. Rev. Lett. 101, 258301.

Ballesta, P., Petekidis, G., Isa, L., Poon, W.C.K., Besseling, R., 2012. Wall slip and flow of concentrated hard-sphere colloidal suspensions. J. Rheol. 56, 1005–1037.

Bertola, V., Bertrand, F., Tabuteau, H., Bonn, D., Coussot, P., 2003. Wall slip and yielding in pasty materials. J. Rheol. 47, 1211–1226.

B, J., Malek, J., Rajagopal, K.R., 2020. On the classification of incompressible fluids and a mathematical analysis of the equations that govern their motion. SIAM J. Math. Anal. 52 (2), 1232–1289. https://doi.org/10.1137/19M1244895. In this issue.

Chaparian, E., Tammisola, O., 2021. Sliding flows of yield stress fluids. J. Fluid Mech. 911, A17.

Clasen, C., 2012. Determining the true slip of a yield stress material with a sliding plate rheometer. Rheol. Acta 51, 883–890.

Cloitre, M, Bonnecaze, R T, 2017. A review on wall slip in high solid dispersions. Rheol. Acta 56, 283–305.

Damianou, Y., Philippou, M., Kaoullas, G., Georgiou, G.C., 2014. Cessation of viscoplastic Poiseuille flow with wall slip. J. Non Newton. Fluid Mech. 203, 24–37.

Damianou, Y., Kaoullas, G., Georgiou, G.C., 2016. Cessation of viscoplastic Poiseuille flow in a square duct with wall slip. J. Non Newton. Fluid Mech. 233, 13–26.

Damianou, Y., Panaseti, P., Georgiou, G.C., 2019. Viscoplastic Couette flow in the presence of wall slip with non-zero slip yield stress. Materials 12 (21), 3574.

Ewoldt, R.H., Johnston, M.T., Caretta, L.M., 2015. Experimental challenges of shear rheology: how to avoid bad data. In: Spagnolie, S. (Ed.), Complex Fluids in Biological Systems. Springer, New York, NY. Biological and medical physics, biomedical engineering(2015).

Hatzikiriakos, S.G., 2012. Wall slip of molten polymers. Prog. Polym. Sci. 37, 624–643.

Hatzikiriakos, S.G., 2015. Slip mechanisms in complex fluid flows. Soft Matter 11, 7851–7856.

Herschel, W., Bulkley, R., 1926. Measurement of consistency as applied to rubber-benzene solutions. Proc. Am. Soc. Test Mater. 26, 621–633.

Hill, D.A., Hasegawa, T., Denn, M.M., 1991. On the apparent relation between adhesive failure and melt fracture. J. Rheol. 34, 891–918.

Jofore, B.D., Erni, P., Vleminckx, G., Moldenaers, P., 2015. Rheology of microgels in single particle confinement. Rheol. Acta 54, 581–600.

Medina-Bañuelos, E.F., Marín-Santibáñez, B.M., Pérez- González, J., Kalyon, D.M., 2017. Tangential annular (Couette) flow of a viscoplastic microgel with wall slip. J. Rheol. 61, 1007–1022.

Meeker, S.P., Bonnecaze, R.T., Cloitre, M., 2004a. Slip and flow in soft particle pastes. Phys. Rev. Lett. 92, 198302.

Meeker, S.P., Bonnecaze, R.T., Cloitre, M., 2004b. Slip and flow in soft particle: direct observation and rheology. J. Rheol. 48, 1295–1320.

Mooney, M., 1931. Explicit formulas for slip and fluidity. J. Rheol. 2, 210–222.

Moud, A.B., Poisson, J., Hudson, Z.M., Hatzikiriakos, S.G., 2021a. Yield stress and wall slip of kaolinite networks. Phys. Fluids 33, 053105.

Moud, A.A., Piette, J., Danesh, M., Georgiou, G.C., Hatzikiriakos, S.G., 2021b. Apparent slip in colloidal suspensions. J. Rheol. submitted.

Navier, C.L.M.H., 1827. Sur les lois du mouvement des fluids. Mem. Acad. R. Sci. Inst. Fr. 6, 389–440.

Poumaere, A., Moyers-González, M., Castelain, C., Burghelea, T., 2014. Unsteady laminar flows of a Crabopol gel in the presence of wall slip. J. Non Newton. Fluid Mech. 205, 28–40.

Schofield, R.K., Scott Blair, G.W., 1931. The influence of the proximity of a solid wall on the consistency of viscous and plastic materials II. J. Phys. Chem. 35, 1505–1508.

Seth, J.R., Cloitre, M., Bonnecaze, R.T., 2008. Influence of short-range forces on wall-slip in microgel pastes. J. Rheol. 52, 1241–1268.

Yoshimura, A., Prud'homme, A.K., 1988. Wall slip corrections for Couette and parallel disk viscometers. J. Rheol. 32, 53–67.